

# Compact high-quality CdSe–CdS core–shell nanocrystals with narrow emission linewidths and suppressed blinking

Ou Chen<sup>1</sup>, Jing Zhao<sup>1</sup>, Vikash P. Chauhan<sup>2</sup>, Jian Cui<sup>1</sup>, Cliff Wong<sup>1</sup>, Daniel K. Harris<sup>1</sup>, He Wei<sup>1</sup>, Hee-Sun Han<sup>1</sup>, Dai Fukumura<sup>2</sup>, Rakesh K. Jain<sup>2</sup> and Mounqi G. Bawendi<sup>1\*</sup>

**High particle uniformity, high photoluminescence quantum yields, narrow and symmetric emission spectral lineshapes and minimal single-dot emission intermittency (known as blinking) have been recognized as universal requirements for the successful use of colloidal quantum dots in nearly all optical applications. However, synthesizing samples that simultaneously meet all these four criteria has proven challenging. Here, we report the synthesis of such high-quality CdSe–CdS core–shell quantum dots in an optimized process that maintains a slow growth rate of the shell through the use of octanethiol and cadmium oleate as precursors. In contrast with previous observations, single-dot blinking is significantly suppressed with only a relatively thin shell. Furthermore, we demonstrate the elimination of the ensemble luminescence photodarkening that is an intrinsic consequence of quantum dot blinking statistical ageing. Furthermore, the small size and high photoluminescence quantum yields of these novel quantum dots render them superior *in vivo* imaging agents compared with conventional quantum dots. We anticipate these quantum dots will also result in significant improvement in the performance of quantum dots in other applications such as solid-state lighting and illumination.**

Nanocrystal quantum dots (QDs) have great potential as a unique optical material in a broad range of applications that rely on downshifting light, especially those relying on achieving spectral purity at high optical flux. These applications include multiplexed labelling and tracking of cells or molecules in a biological environment<sup>1–4</sup>, downshifting light for colour engineering in solid-state lighting, illumination and displays<sup>5–7</sup>, and single-photon sources<sup>8–10</sup>. To fully realize the potential of QDs in this broad class of applications, the following criteria, which may not be strictly independent, need to be simultaneously fulfilled: high particle uniformity, high photoluminescence quantum yields (QYs) for optimized brightness, narrow and symmetric emission spectra for multiplexing and colour saturation, and minimized single-QDs blinking for tracking and for light output stability. Also, applications in biological environments generally require the QDs to be as compact as possible to minimize interactions with biological systems and to maximize diffusion to confined biological spaces of interests<sup>11</sup>.

In the past two decades, significant progress has been made in synthesizing QDs with uniform size, high photoluminescence QYs and narrow emission spectra<sup>12,13</sup>. However, these QDs display significant ‘blinking’, whereby the photoluminescence of single-QDs turns ON and OFF under continuous excitation, which limits the use of QDs in tracking applications, as single-photon sources and in downshifting illumination applications at relatively high fluxes<sup>14–16</sup>. Recently, a few groups have reported successes towards non-blinking or nearly non-blinking QDs (refs 17–22). So far, two general approaches have been developed towards suppressing blinking. The first approach relies on changing the solution environment of the QDs by adding ‘antiblinking agents’

that presumably bind to the QD surface<sup>17–19</sup>. However, this blinking suppression is not an intrinsic property of the QDs and relies on weakly bound surface species so that the initial blinking state is easily and almost immediately recovered by displacement of the antiblinking agent<sup>17,18</sup>. This lack of robustness and the requirement of the QDs being in a solution containing an excess of the antiblinking agent are unacceptable for most applications<sup>1–4</sup>. The second approach is to grow a thick inorganic shell (>5 nm) on the QDs to fully isolate the excited carriers from the QD surface and the surface environment<sup>20,21</sup>. However, these ‘giant’ core–shell QDs are often large, with a poor size distribution, have a broad photoluminescence spectra, with only moderate ensemble photoluminescence QYs (refs 20,21). Therefore, synthesizing QDs that simultaneously satisfy all criteria discussed above has not yet been possible.

We have met the challenge here through a novel synthesis that produces high-quality CdSe–CdS core–shell QDs using cadmium (II) oleate (Cd-oleate) and octanethiol as shell precursors. Owing to the strong carbon–sulphur chemical bond in octanethiol, the shell-growth temperature is at 310 °C. The slow continuous shell precursor infusion and the relatively low reactivity of octanethiol provide an optimal condition, leading to a well-maintained particle size distribution during shell growth. Because of the small lattice mismatch (3.9%) between core and shell and the slow, high-temperature growth, the resulting QDs maintain the original crystal structure of the CdSe core. In contrast with previous observations, we find that single-QDs blinking is significantly suppressed with only a relatively thin shell (~2.4 nm, ~7 monolayers; MLs). Consequently, the intrinsic ensemble photoluminescence photodarkening induced by blinking statistical ageing is eliminated,

<sup>1</sup>Department of Chemistry, Massachusetts Institute of Technology, 77 Massachusetts Avenue, Cambridge, Massachusetts 02139, USA, <sup>2</sup>Massachusetts General Hospital and Harvard Medical School, 100 Blossom Street, Boston, Massachusetts 02114, USA. \*e-mail: [mgb@mit.edu](mailto:mgb@mit.edu).

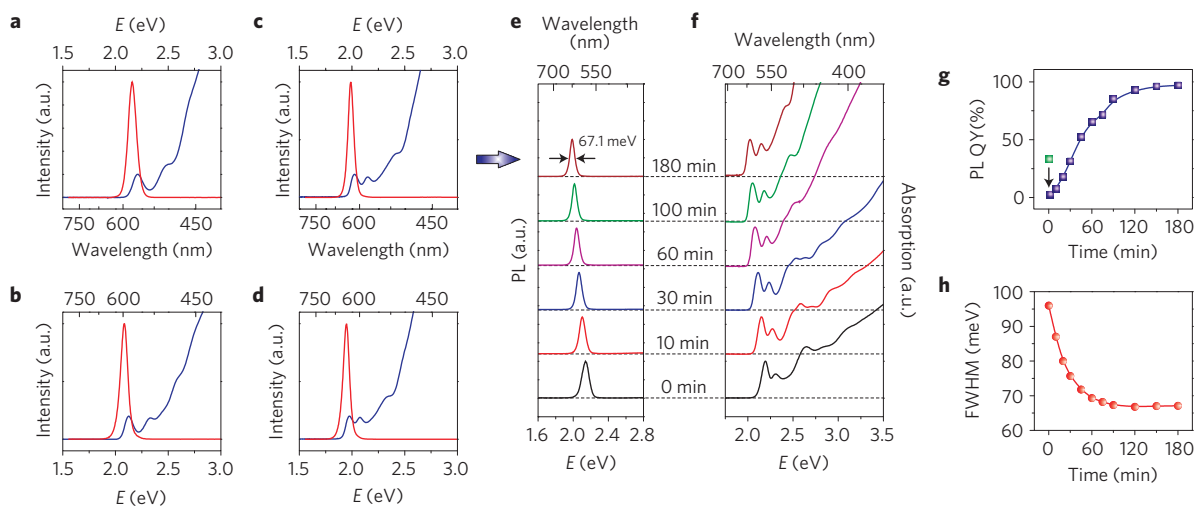


**Figure 1 | Optical properties of new generation CdSe–CdS core-shell QDs.** **a–d**, Absorption (blue) and photoluminescence (PL) (red) spectra of four different CdSe–CdS core-shell QDs synthesized with different CdSe core diameters of 2.7 nm (**a**), 3.4 nm (**b**), 4.4 nm (**c**) and 5.4 nm (**d**). **e–h**, Temporal evolution of photoluminescence (PL, **e**), absorption (**f**), photoluminescence QYs (**g**), green square shows the original photoluminescence QY of CdSe QDs, and FWHM of the photoluminescence peak of the CdSe–CdS core-shell QDs (shown in **c**) during the shell growth reaction (**h**).

making these QDs stable ensemble photoluminescence output sources even at relatively high optical fluxes. Most importantly, this new generation of QDs for the first time simultaneously satisfies the four criteria of high uniformity, high photoluminescence QYs (up to 97%), narrow photoluminescence peaks (full-width at half-maximum (FWHM) as narrow as 67.1 meV ( $\sim 20$  nm)), and significantly suppressed blinking ( $\sim 94\%$  average ON time fractions). Furthermore, this thin shell allows for compact QDs suitable for biological imaging applications. These QDs can be easily brought into water maintaining the high photoluminescence QYs ( $>70\%$ ) desired for imaging probes in highly scattering biological environments. This new generation of QDs will result in significant performance improvements in a variety of applications ranging from solid-state lighting, illumination and displays to biological multiplexed labelling and tracking.

Absorption and photoluminescence spectra of four CdSe–CdS QDs samples synthesized by our method are shown in Fig. 1a–d. Cd-oleate and octanethiol were chosen as the shell precursors. The low reactivity induced by the strong carbon–sulphur covalent bond in octanethiol requires a relatively high temperature ( $310^\circ\text{C}$ ) for shell growth. During the overcoating reaction (Supplementary Information), both the photoluminescence peak and the absorption features shift to lower energy (Fig. 1e,f) as a consequence of the weak exciton confinement generated by the CdS shell<sup>23</sup>. Narrow and symmetric photoluminescence peaks and absorption spectra with well-resolved transitions indicate that particle size distributions remain tight throughout the entire shell-growth process (Fig. 1e,f). Photoluminescence QY measurements show that after an initial drop, due to quenching by the addition of octanethiol (Fig. 1g)<sup>24,25</sup>, the photoluminescence QY monotonically increases during the reaction and reaches its maximum when the reaction solution is annealed at  $310^\circ\text{C}$  for 60 min following precursors injection (Fig. 1g). The photoluminescence QYs of the obtained QDs were observed to be as high as 97%. The photoluminescence peak FWHM decreases greatly from 96.2 meV for ‘bare’ CdSe QDs to 67.1 meV ( $\sim 20$  nm) for final CdSe–CdS QDs (Fig. 1h), consistent with the decreased half-width at half-maximum of the first absorption peak (Supplementary Fig. S3). Remarkably, this uniquely narrow ensemble photoluminescence peak width (67.1 meV) is comparable to that from single-QDs (50–70 meV; ref. 26). To the best of our knowledge, such a narrow and symmetric ensemble emission peak has not been

achieved before for any CdSe-based core–shell or alloy QDs. This narrow ensemble photoluminescence can enhance the spectral purity of QD-based illumination or display applications, and enables an increased number of wavelength detection channels in multiplexing applications.

Transmission electron microscopy (TEM) measurements show that, during CdS shell growth, the average particle diameter increases from 4.4 to 9.1 nm, which corresponds to a shell thickness of 2.4 nm ( $\sim 7$  MLs; Fig. 2a–d and Supplementary Fig. S5; ref. 27). The size distribution of the core–shell QDs remains exceptionally narrow ( $\sim 4\%$ ) during the entire shell-growth process (Fig. 2a–d and Supplementary Fig. S5), consistent with optical measurements (Fig. 1). This narrow size distribution may be due to the slow shell precursor infusion and the low reactivity of the octanethiol, which may provide a constant and sufficient monomer production rate, consistent with a recent model<sup>28</sup>. Energy-dispersive X-ray spectroscopy shows that the atomic percentages of Cd, Se and S atoms are in good agreement with the calculated values based on the CdSe core size and CdS shell thickness determined by TEM (Fig. 2e). High-resolution TEM images reveal high crystallinity with lattice fringes throughout the whole particle (Fig. 2f, inset and Supplementary Fig. S7). The shown lattice distance of 3.64 Å (Fig. 2f, inset) corresponds to the (100) lattice spacing of the wurtzite (W) crystal structure. XRD results confirm a W crystal structure with characteristic (102) and (103) Bragg peaks (Fig. 2f), in agreement with the W crystal structure of the starting cores, demonstrating epitaxial shell formation. To further confirm this epitaxial shell growth, W–CdSe cores were replaced with zinc-blende (ZB) CdSe cores. As expected, the resulting particles show a ZB crystal structure (Supplementary Fig. S8; ref. 29). This observation is in contradiction with recent results that the CdS shell growth on ZB–CdSe QDs in the presence of primary amines (that is, oleylamine) necessarily generates core–shell particles simultaneously containing both W and ZB crystal structures<sup>20,30</sup>. We believe that in our case, the slow shell growth maintains the original crystal structure of the starting core material. Moreover, these results are in accordance with the recent finding of ZB–CdSe–CdSe iso-material core–shell growth<sup>31</sup>.

As shown in Fig. 1, the photoluminescence peak of the final core–shell QDs is remarkably narrow (FWHM: 67.1 meV,  $\sim 20$  nm), comparable to single-QDs emission linewidths<sup>26</sup>. Such uniquely narrow and symmetric ensemble emission peaks are desired in

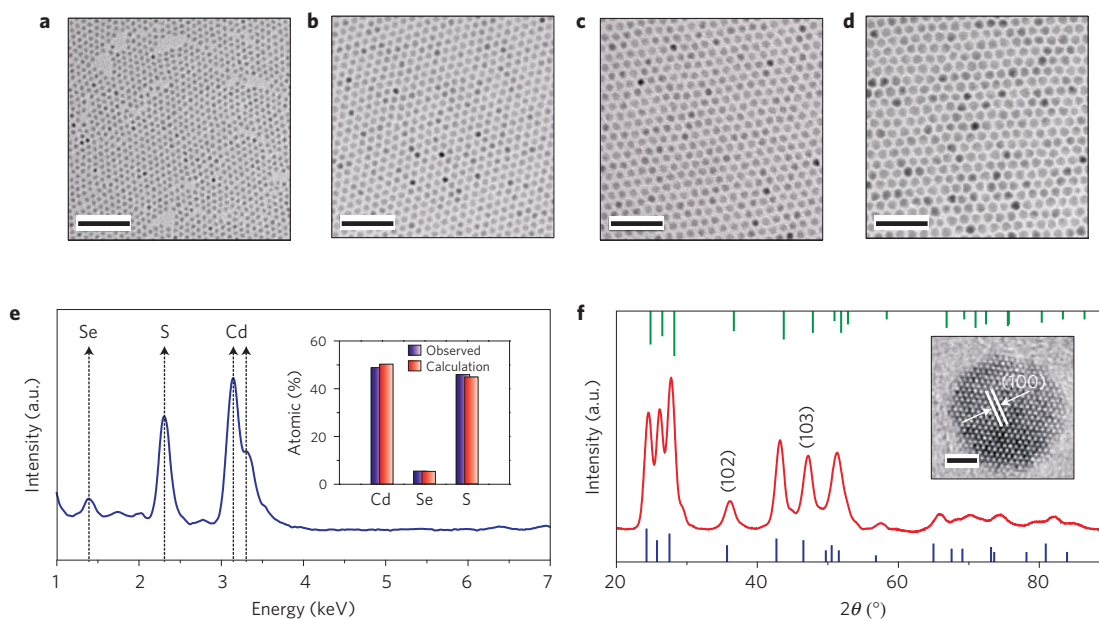


**Figure 2 | Morphology, composition and crystal structure characterization of new generation QDs. a–d,** TEM images of 4.4 nm CdSe core (a) and CdSe–CdS core-shell QDs with a CdS shell thickness of 0.8, 1.6 and 2.4 nm, respectively (b–d). **e,** Energy-dispersive X-ray spectrum of the final CdSe–CdS core-shell QDs shown in d. Inset shows the observed and calculated atomic percentages of Cd, Se and S atoms. **f,** X-ray powder diffraction pattern measured from the same sample shown in d. The stick patterns show the standard peak positions of bulk wurtzite CdSe (bottom blue sticks) and CdS (top green sticks). The inset shows a representative high-resolution TEM image of a CdSe–CdS QD. Scale bars, 50 nm in a–d and 2 nm in the inset of f.

many applications. Exploring the origins of this narrow emission peak is therefore intriguing.

We can consider two possible scenarios: the average photoluminescence peak width of single-QDs synthesized here is narrower than that of single-QDs synthesized by other methods, resulting in a narrower ensemble photoluminescence peak; or the narrow ensemble emission peak comes from the high sample uniformity, minimizing inhomogeneous broadening from size/morphology distributions. To examine these hypotheses, we carried out emission linewidth measurements for single-QDs as well as for the ensemble using photon correlation Fourier spectroscopy in solution (S-PCFS; refs 32,33). The average single-QDs and ensemble spectral correlations for our core-shell QDs are shown in Fig. 3a. After fitting (Supplementary Information), the ensemble emission FWHM is 69 meV, nearly identical to that obtained using a spectrometer (Fig. 1e,h). The average single-QD emission FWHM is 63 meV, in good agreement with previous studies<sup>26,32</sup>. The small difference (6 meV, ~10%) between the single-QDs and the ensemble emission linewidths indicates extremely high uniformity of the sample, including uniform shape, narrow size distribution, high shell crystallinity, sufficient surface passivation, and so on. These results confirm the hypothesis of the first scenario—that this narrow ensemble photoluminescence peak is due to the high uniformity of our QDs—rather than unusually narrow single-QD photoluminescence peaks.

For comparison, the emission linewidth of the CdSe–CdS QDs synthesized using a conventional method<sup>23</sup> was also measured using S-PCFS (Fig. 3b). Fitting results show that the average single-QDs emission FWHM is 65 meV. However, the ensemble emission linewidth is 111 meV (~34 nm), ~60% broader than our QDs, indicating a relatively polydisperse sample. TEM measurements show two indications of increased polydispersity: broader particle size distribution (~6%) and irregular shapes (Supplementary Fig. S10). Other factors not observed in TEM, such as a polydispersity in surface structure, insufficient surface passivation, and increased spectral diffusion may also be contributing factors to this broader ensemble linewidth.

Ever since single-QDs fluorescence intermittency has been discovered<sup>14–16,34,35</sup>, it has been recognized as a potential limitation of QDs in a variety of applications. For example, the existence of long OFF periods (for example, tens of seconds or longer) hinders the use of QDs in biological settings for tracking. Blinking also limits the potential use of QDs as single-photon sources. In another example, the power-law distribution associated with OFF times at the single-QDs level results in an intrinsic ensemble photoluminescence photodarkening when the dots are continuously excited with a high flux<sup>36,37</sup>. This intrinsic photodarkening limits QDs from being a stable photoluminescence output source under high flux excitation, such as in solid-state lighting and low-threshold lasers. QDs with suppressed blinking are therefore attractive across a broad class of applications.

To further characterize our QDs at the single-emitter level, we studied single-QDs blinking behaviour using a CdSe–CdS QDs sample with a shell thickness of 2.4 nm (~7 ML). Figure 4a shows a representative photoluminescence blinking trace and histogram of photoluminescence intensity distributions. The antibunching dip ( $\tau = 0$ ) from a second-order photon intensity correlation ( $g^{(2)}(\tau)$ ) measurement is consistent with the expected emission from a single-QD and not a cluster of QDs (Supplementary Fig. S11; ref. 38). Some antibunching ‘dips’ do not drop to the background level (Supplementary Fig. S13), owing to the heterogeneity of bi-exciton QYs recently observed<sup>38–40</sup>. This heterogeneity in bi-exciton QYs does not affect our observed blinking traces because of the negligible bi-exciton population under our experimental conditions<sup>38</sup>. Figure 4a shows well-resolved ON–OFF blinking. An average time fraction that the QDs stay ON during the course of the measurements was extracted from 135 blinking traces each from a different QD, with the resulting distribution shown in Fig. 4b. The average ON time fraction is ~94% and ~20% of the QDs we studied exhibited an ON time fraction greater than 99% (Fig. 4b). Note that ‘grey states’ which have been observed and attributed to the emission from a positive trion have not been observed here<sup>41</sup>. This indicates that deep electron or hole traps are significantly eliminated, consistent with the high ON time fraction measured for exciton emission.

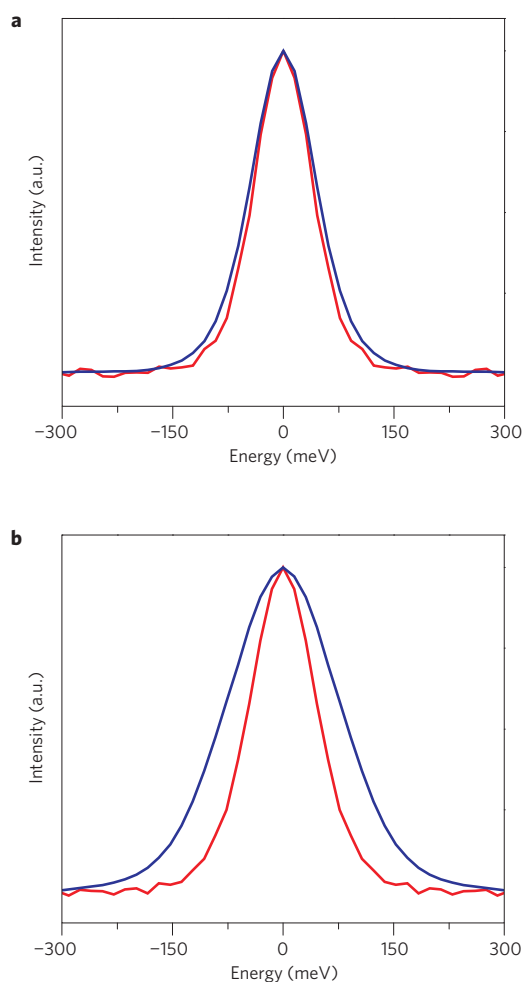


**Figure 3 | Photoluminescence spectral correlation of single-QDs and ensemble QDs obtained through S-PCFS. a,b**, The spectral correlations of the single-QD (red line) and the ensemble (blue line) spectrum obtained by S-PCFS for CdSe–CdS core–shell QDs synthesized by our method (**a**) and a conventional method with nearly the same shell thickness ( $\sim 7$  MLs; **b**).

The statistics of ON and OFF times calculated from the blinking traces are plotted in Fig. 4c. The probability distributions for the duration of ON and OFF events  $P_{\text{on/off}}$ , fit power-law distributions  $P_{\text{on/off}}(t_{\text{on/off}} \propto t^{-\alpha_{\text{on/off}}})$ , where  $t_{\text{on/off}}$  are the time intervals for a QD in an ON or OFF state, and  $\alpha_{\text{on/off}}$  are the power-law exponents expressing the statistics of ON–OFF events. For our core–shell QDs,  $\alpha_{\text{on}} = 0.85$  and  $\alpha_{\text{off}} = 2.2$ . Note that usually both  $\alpha$  values for CdSe/ZnS QDs are close to 1.5 (refs 16,36,37,42,43). The slow decay of the ON time distribution and fast decay of the OFF time distribution indicate that photoluminescence blinking is dominated by long ON events and short OFF events, consistent with the observed high ON time fraction. These exponents describe distributions of ON and OFF times that are qualitatively different from the usual ones and, as discussed below, predict an ensemble behaviour that is also qualitatively different.

Recent work shows that the blinking of CdSe–CdS QDs can be greatly suppressed by growing thick CdS shells ( $>5$  nm,  $\sim 15$  MLs), which effectively isolate the excited carriers from the nanocrystal surface and surrounding environment<sup>20,21</sup>. Recently, single-QDs blinking suppression has been correlated with particle volume<sup>44</sup>. It has been claimed that to observe suppressed blinking from single CdSe–CdS QDs, the final single particle volume must be no less than  $\sim 750$  nm<sup>3</sup>, with a radiative lifetime of  $\sim 65$  ns or longer<sup>44</sup>. However, the single-particle volume of our QDs is only

about half of their threshold volume ( $\sim 390$  nm<sup>3</sup>) with a much shorter photoluminescence lifetime of  $\sim 32$  ns (Supplementary Fig. S12). Our results strongly suggest that, even with a relatively thin shell, the blinking behaviour of core–shell QDs can be qualitatively altered by improved synthetic methodology. We speculate that the significantly reduced blinking observed here is at least partially caused by a highly crystalline shell that results from high-temperature slow shell-growth conditions.

To prove this hypothesis, we synthesized CdSe–CdS QDs with a very thin shell ( $\sim 0.7$  nm,  $\sim 2$  MLs) through our method and characterized their blinking properties. The calculated ON time fraction of 85% (Fig. 4d and Supplementary Fig. S14) is very much higher than that of CdSe–CdS QDs with similar shell thicknesses synthesized using more common methods<sup>20,44–46</sup>. As a result of this thin shell and small conduction bands offset (0.29 eV) between the core and shell<sup>47</sup>, the excited carrier (that is, an electron) is delocalized in the entire particle and easily access the particle surface. Thus, the greatly increased ON time fraction we observe for this sample cannot be explained by the physical separation between the excited carriers and the nanocrystal surface and surrounding environment, as is usually the case for thick shell ( $>5$  nm) QDs (refs 20,21). Therefore, we speculate that this improvement in blinking behaviour is a consequence of the high shell crystallinity that results through controllable and relatively slow CdS epitaxial shell formation. The use of the relatively stable octanethiol precursor provides shell precursor atoms at a slow growth rate, allowing for annealing of the shell structure and the surface during growth, minimizing defects at interfaces, within the shell and on the surface (for example, stacking faults, vacancies, dislocation, dangling bonds and so on) which could initiate fast non-radiative decays and turn the particle OFF<sup>14,15,20,21,34</sup>. This explanation is consistent with the crystal structure study discussed above as well as the ligand-exchange results shown below. Furthermore, our results also demonstrate that shell thickness still does play a role in controlling single-QDs blinking, consistent with previous observations<sup>20,44,45</sup>, but with a significantly thinner shell.

Photodarkening effects from collections of QDs (the ensemble level) that are exclusively caused by statistical ageing from single-QDs blinking have been both experimentally observed and theoretically modelled<sup>36,37</sup>. In contrast to photochemical degradation (for example, permanent photochemical darkening), this ensemble photoluminescence intensity decay is intrinsic, inevitable, and reversible, because it is purely induced by the non-ergodicity of single-QDs blinking distributions, as expected from Lévy statistics, where the mean and variance of the distributions diverge<sup>48</sup>. When ON and OFF events share the same or similar power-law distributions, as is the usual case, but with the ON time distribution truncated, as time progresses, long OFF states become dominant and the ensemble photoluminescence decays. However, the QDs studied here exhibit a qualitatively and statistically different blinking behaviour with significantly different ON and OFF powers (0.85 versus 2.2) (Fig. 4c), compared with the usual observations where both ON and OFF powers are close to  $\sim 1.5$  with a short ON time cut-off<sup>36,37</sup>. Rather than being dominated by the OFF times, as is traditionally the case, our samples are now dominated by the ON times, with significant implications for ensemble photoluminescence stabilities. To explore the photoluminescence stability of our novel QDs at the ensemble level, a collection of QDs was excited by a continuous wave laser at 514 nm under the same excitation flux as used for previous single-QDs blinking studies (that is,  $80$  W cm<sup>-2</sup>). After slightly photobrightening (photoluminescence intensity increases  $\sim 8\%$ , Fig. 4e), the photoluminescence intensity stays constant during the course of the measurement ( $\sim 7.2 \times 10^4$  s). This observation is consistent with the fast decay of the OFF time distribution and the slow decay of the ON time distribution (Fig. 4c), as well as the calculation of the ON



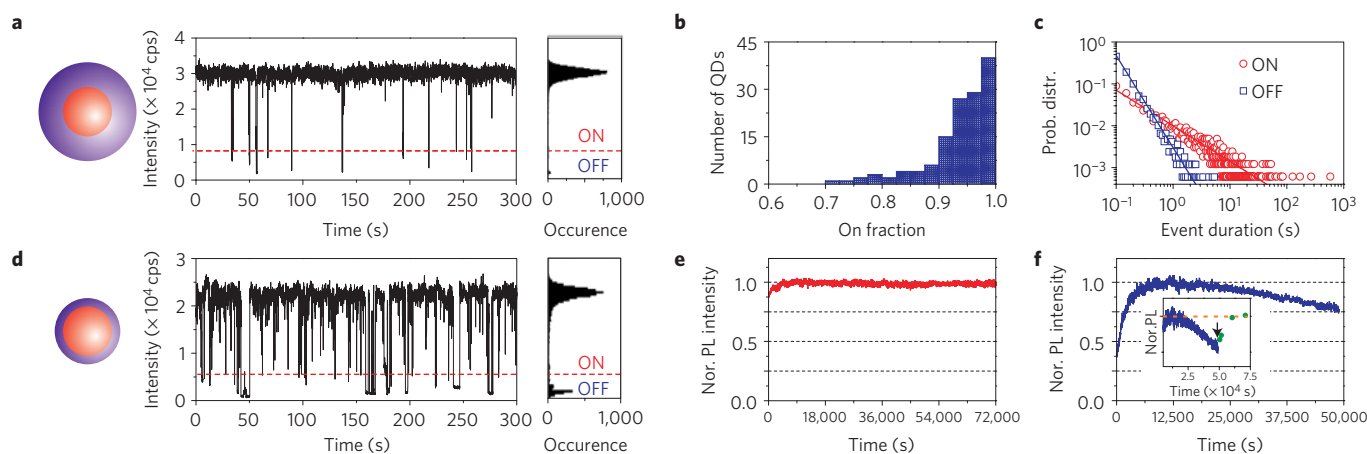


**Figure 4 | Blinking behaviour of new generation CdSe–CdS core–shell QDs and ensemble photoluminescence stability test.** **a**, Representative photoluminescence blinking trace of a single CdSe–CdS core–shell QD with a CdSe core radius of 2.2 nm and a shell thickness of 2.4 nm (~7 MLs; bin size is 50 ms). Histograms indicate the distribution of intensities observed in the trace. The dashed red line indicates the value chosen as the threshold between ON and OFF states in calculating the ON time fraction. **b**, Histogram of the blinking ON time fraction. The average ON time fraction is 0.94 with a standard deviation of  $\pm 0.06$ . **c**, Log–log plot of the probability distributions of ON and OFF times. Straight lines represent a power-law fitting using the equation  $P_{\text{on/off}}(t_{\text{on/off}}) \propto t^{-\alpha_{\text{on/off}}}$ , where  $\alpha_{\text{on}} = 0.85$  for ON times (red line) and  $\alpha_{\text{off}} = 2.2$  for OFF times (blue line). **d**, Representative photoluminescence blinking trace of a single CdSe–CdS core–shell QD with a CdSe core radius of 2.2 nm and a shell thickness of 0.7 nm (~2 MLs; bin size is 50 ms). **e, f**, The normalized (Nor.) photoluminescence intensity traces obtained from a collection of QDs synthesized through our new method (**e**) and the conventional method (**f**). The inset in **f** shows the photoluminescence intensity recovery after an initial decay. The black arrow indicates the time point when continuous excitation was stopped.

time distribution dominated ensemble photoluminescence QYs evolution (Supplementary Information). A cut-off time for this ON time distribution, which may not be easily accessible even for the measurement at the ensemble level (Fig. 4e), is very likely to exist. As a control experiment, the ensemble photoluminescence intensity trace collected from a collection of CdSe–CdS QDs that were synthesized through a more conventional method with ‘normal’ power-law blinking behaviour (Supplementary Fig. S16) is plotted in Fig. 4f. It reveals that after an initial photobrightening process, the ensemble photoluminescence intensity begins to decrease after  $\sim 2 \times 10^4$  s, implying a truncation of the ON time distribution at  $\sim 2 \times 10^4$  s, (a timescale inaccessible with single-QDs measurements; Supplementary Fig. S16; ref. 37). The photoluminescence intensity decreases  $\sim 23\%$  from its highest value under continuous excitation of  $\sim 5 \times 10^4$  s (Fig. 4f). These results are in good agreement with previous observations<sup>36,37</sup>. Complete photoluminescence recovery after removal of the excitation (Fig. 4f, inset) is consistent with this photodarkening originating from single-QDs blinking statistical ageing, and not an irreversible photochemical degradation process<sup>36,37</sup>. This result is also consistent with an initial photobrightening process that is irreversible and probably caused by neutralizing initially charged QDs, as has been previously observed<sup>49</sup>.

Fluorescent organic dyes are commonly used for both *in vitro* assay detections and *in vivo* imaging applications<sup>50</sup>; nonetheless, their intrinsic characteristics of broad/asymmetric emission profiles, significant blinking, low absorption cross sections, and low photobleaching thresholds limit their performance in long-term and/or multiplexing imaging studies<sup>3,48</sup>. The QDs presented here with high photoluminescence QYs, narrow emission peak and suppressed blinking, render them ideal for ultrasensitive and multiplexing investigations in the broad biomedical domain<sup>3,8</sup>. Furthermore, in an advance over prior non-blinking QDs (refs 20,21), our new generation (ng) QDs are small and compact, which allows them to be accessible to confined biological spaces of interest<sup>11</sup>. To demonstrate the benefit of using our QDs for *in vivo* imaging, two samples underwent the same ligand-exchange reaction (Supplementary Information): conventional CdSe–CdS QDs ( $\text{QD}_{\text{conv.}}$ ) with a photoluminescence QY of 43%; our new generation CdSe–CdS QDs ( $\text{QD}_{\text{ng}}$ ) with

a photoluminescence QY of 94%. Both samples were successfully transferred into aqueous solution via a ligand-exchange reaction with methoxy-polyethylene-glycol thiol (PEG–SH, MW5000). Hydrodynamic diameters for PEG–SH capped  $\text{QD}_{\text{conv.}}$ –SH–PEG and  $\text{QD}_{\text{ng}}$ –SH–PEG are 18.3 nm and 18.7 nm, respectively (Supplementary Fig. S17), indicating no measurable aggregation<sup>11</sup>. After ligand-exchange, the photoluminescence QY decreased to 13% ( $\sim 70\%$  quenching) for  $\text{QD}_{\text{conv.}}$ –SH–PEG, and to 71% ( $\sim 24\%$  quenching) for  $\text{QD}_{\text{ng}}$ –SH–PEG (Fig. 5a,b). Thiol groups have been shown to generally quench the photoluminescence through QD surface trap states<sup>24,25</sup>. The different photoluminescence QY quenching levels between these two samples reflect a qualitative difference in surface passivation. Our QDs ( $\text{QD}_{\text{ng}}$ ) showed much less quenching, suggesting better passivation.

To demonstrate the consequence of this improvement, we imaged  $\text{QD}_{\text{conv.}}$ –SH–PEG and  $\text{QD}_{\text{ng}}$ –SH–PEG *in vivo*. We intravenously injected these QDs at equal concentrations (2.5  $\mu\text{M}$ ) into Tie2-GFP transgenic mice bearing dorsal skinfold chambers, and carried out intravital multiphoton microscopy in the skin (Fig. 5d,e; ref. 51). The *in vivo* fluorescence signal of  $\text{QD}_{\text{ng}}$ –SH–PEG was  $\sim 4.7$  times more intense than that of  $\text{QD}_{\text{conv.}}$ –SH–PEG (Fig. 5d,e and Supplementary Fig. S18). Importantly, these results roughly matched the difference in QYs for these QDs (Fig. 5a,b), indicating this improved photoluminescence QYs translates to enhanced brightness for *in vivo* imaging applications.

Furthermore, similar to what we observed before<sup>11,52</sup>, polymeric imidazole ligands (PILs) capped ng-QDs ( $\text{QD}_{\text{ng}}$ –PIL) show a smaller hydrodynamic diameter ( $\sim 15.6$  nm; Supplementary Fig. S17), higher photoluminescence QY in PBS (77%) (Fig. 5c) and brighter in *in vivo* imaging ( $\sim 20\%$  more intense; Fig. 5f and Supplementary Fig. S18) than using  $\text{QD}_{\text{ng}}$ –SH–PEG under the same experimental conditions.

In summary, we have successfully synthesized high-quality CdSe–CdS core–shell QDs using Cd-oleate and octanethiol as shell precursors at a relatively high temperature of 310 °C. We find that, for core–shell QDs with relatively thin shells ( $\sim 2.4$  nm), blinking from single-QDs is significantly suppressed. Consequently, the intrinsic ensemble photoluminescence photodarkening induced

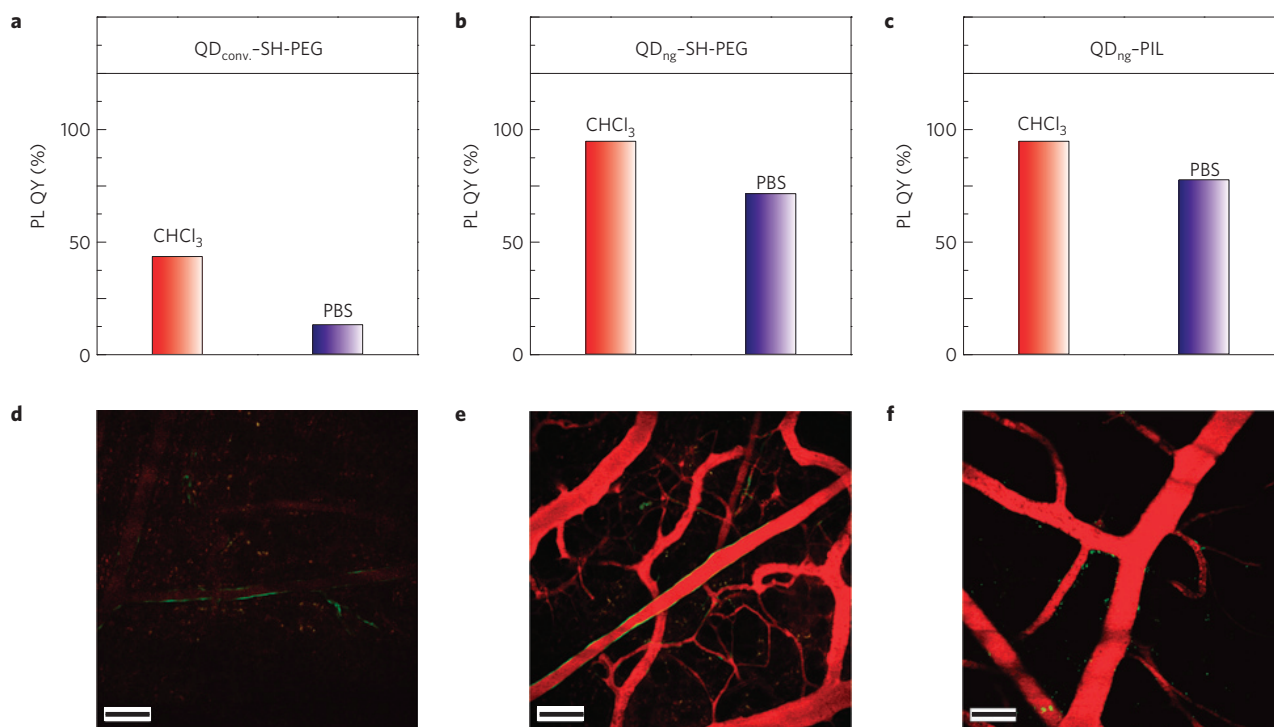


**Figure 5 | Water-soluble CdSe-CdS core-shell QDs for *in vivo* imaging.** **a-c**, Photoluminescence QYs of CdSe-CdS core-shell QDs before ligand exchange in chloroform (CHCl<sub>3</sub>) and after ligand exchange in phosphate buffer saline (PBS 1X, pH 7.4). Equal amounts of these QDs (2.5 μM, 200 μl) were injected retro-orbitally into Tie2-GFP transgenic mice bearing dorsal skinfold chambers, and carried out intravital multiphoton microscopy in the skin at 30 min after injection. **d-f**, The multiphoton *in vivo* images. **a,d**, Conventional CdSe-CdS QDs synthesized by a literature method and ligand exchanged with methoxy-polyethylene-glycol thiol (QD<sub>conv.</sub>-SH-PEG). **b,e**, New generation (ng) CdSe-CdS QDs synthesized by our novel method and ligand exchanged with methoxy-polyethylene-glycol thiol (QD<sub>ng</sub>-SH-PEG). **c,f**, New generation CdSe-CdS QDs ligand exchanged with polymeric imidazole ligands (QD<sub>ng</sub>-PIL). In **d-f**, all the images are scaled to the same contrast, and scale bars, 100 μm.

by statistical ageing from blinking under long time excitation is eliminated. Most importantly, these core-shell QDs simultaneously satisfy all four criteria, including high uniformity, high photoluminescence QYs, narrow emission peaks, and significantly suppressed blinking. Moreover, the relatively thin shell allows for compact QDs generally suitable for biological applications. We demonstrate that these core-shell QDs can be easily solubilized into water with high photoluminescence QYs, rendering them promising for *in vivo* imaging. We anticipate that this new generation of QDs will result in significant improvements in a variety of applications, ranging from solid-state lighting and illumination under high and/or long time flux and single-photon generation, to biological multiplexed labelling, real-time tracking and *in vivo* transport studies.

Received 6 August 2012; accepted 4 December 2012;  
published online 3 February 2013

## References

- Dahan, M. *et al.* Diffusion dynamics of glycine receptors revealed by single-quantum dot tracking. *Science* **302**, 442–445 (2003).
- Stroh, M. *et al.* Quantum dots spectrally distinguish multiple species within the tumour milieu *in vivo*. *Nature Med.* **11**, 678–682 (2005).
- Chan, W. C. W. *et al.* Luminescent quantum dots for multiplexed biological detection and imaging. *Curr. Opin. Biotechnol.* **13**, 40–46 (2002).
- Jaiswal, J. K. & Simon, S. M. Potentials and pitfalls of fluorescent quantum dots for biological imaging. *Trends Cell Biol.* **14**, 497–504 (2004).
- Colvin, V. L., Schlamp, M. C. & Alivisatos, A. P. Light-emitting diodes made from cadmium selenide nanocrystals and a semiconducting polymer. *Nature* **370**, 354–357 (1994).
- Jang, H. S. *et al.* White light-emitting diodes with excellent colour rendering based on organically capped CdSe quantum dots and Sr<sub>3</sub>SiO<sub>5</sub>: Ce<sup>3+</sup>, Li<sup>+</sup> phosphors. *Adv. Mater.* **20**, 2696–2702 (2008).
- Lim, J. *et al.* Preparation of highly luminescent nanocrystals and their application to light-emitting diodes. *Adv. Mater.* **19**, 1927–1932 (2007).
- Resch-Genger, U., Grabolle, M., Cavaliere-Jaricot, S., Nitschke, R. & Nann, T. Quantum dots versus organic dyes as fluorescent labels. *Nature Methods* **5**, 763–775 (2008).
- Brokmann, X., Giacobino, E., Dahan, M. & Hermier, J. P. Highly efficient triggered emission of single photons by colloidal CdSe/ZnS nanocrystals. *Appl. Phys. Lett.* **85**, 712–714 (2004).
- Fisher, B., Caruge, J. M., Zehnder, D. & Bawendi, M. Room-temperature ordered photon emission from multiexciton states in single CdSe core-shell nanocrystals. *Phys. Rev. Lett.* **94**, 087403 (2005).
- Popovic, Z. *et al.* A nanoparticle size series for *in vivo* fluorescence imaging. *Angew. Chem. Int. Ed.* **49**, 8649–8652 (2010).
- Reiss, P., Protiere, M. & Li, L. Core/shell semiconductor nanocrystals. *Small* **5**, 154–168 (2009).
- Jun, S., Jang, E. J. & Chung, Y. S. Alkyl thiols as a sulphur precursor for the preparation of monodisperse metal sulphide nanostructures. *Nanotechnology* **17**, 4806–4810 (2006).
- Nirmal, M. *et al.* Fluorescence intermittency in single cadmium selenide nanocrystals. *Nature* **383**, 802–804 (1996).
- Kuno, M. *et al.* Fluorescence intermittency in single InP quantum dots. *Nano Lett.* **1**, 557–564 (2001).
- Frantsuzov, P., Kuno, M., Janko, B. & Marcus, R. A. Universal emission intermittency in quantum dots, nanorods and nanowires. *Nature Phys.* **4**, 519–522 (2008).
- Hohng, S. & Ha, T. Near-complete suppression of quantum dot blinking in ambient conditions. *J. Am. Chem. Soc.* **126**, 1324–1325 (2004).
- Fomenko, V. & Nesbitt, D. J. Solution control of radiative and nonradiative lifetimes: A novel contribution to quantum dot blinking suppression. *Nano Lett.* **8**, 287–293 (2008).
- Hammer, N. I. *et al.* Coverage-mediated suppression of blinking in solid state quantum dot conjugated organic composite nanostructures. *J. Phys. Chem. B* **110**, 14167–14171 (2006).
- Mahler, B. *et al.* Towards non-blinking colloidal quantum dots. *Nature Mater.* **7**, 659–664 (2008).
- Chen, Y. *et al.* ‘Giant’ multishell CdSe nanocrystal quantum dots with suppressed blinking. *J. Am. Chem. Soc.* **130**, 5026–5027 (2008).
- Wang, X. *et al.* Non-blinking semiconductor nanocrystals. *Nature* **459**, 686–689 (2009).

23. Li, J. J. *et al.* Large-scale synthesis of nearly monodisperse CdSe/CdS core/shell nanocrystals using air-stable reagents via successive ion layer adsorption and reaction. *J. Am. Chem. Soc.* **125**, 12567–12575 (2003).
24. Munro, A. M., Jen-La Plante, I., Ng, M. S. & Ginger, D. S. Quantitative study of the effects of surface ligand concentration on CdSe nanocrystal photoluminescence. *J. Phys. Chem. C* **111**, 6220–6227 (2007).
25. Wuister, S. F., Donega, C. D. & Meijerink, A. Influence of thiol capping on the exciton luminescence and decay kinetics of CdTe and CdSe quantum. *J. Phys. Chem. B* **108**, 17393–17397 (2004).
26. Gomez, D. E., van Embden, J. & Mulvaney, P. Spectral diffusion of single semiconductor nanocrystals: The influence of the dielectric environment. *Appl. Phys. Lett.* **88**, 154106 (2006).
27. Van Embden, J., Jasieniak, J. & Mulvaney, P. Mapping the optical properties of CdSe/CdS heterostructure nanocrystals: The effects of core size and shell thickness. *J. Am. Chem. Soc.* **131**, 14299–14309 (2009).
28. Clark, M. D., Kumar, S. K., Owen, J. S. & Chan, E. M. Focusing nanocrystal size distributions via production control. *Nano Lett.* **11**, 1976–1980 (2011).
29. Chen, O. *et al.* Synthesis of metal-selenide nanocrystals using selenium dioxide as the selenium precursor. *Angew. Chem. Int. Ed.* **47**, 8638–8641 (2008).
30. Mahler, B. D., Lequeux, N. & Dubertret, B. Ligand-controlled polytypism of thick-shell CdSe/CdS nanocrystals. *J. Am. Chem. Soc.* **132**, 953–959 (2010).
31. Chen, O. *et al.* Surface-functionalization-dependent optical properties of II–VI semiconductor nanocrystals. *J. Am. Chem. Soc.* **133**, 17504–17512 (2011).
32. Marshall, L. F., Cui, J., Brokmann, X. & Bawendi, M. G. Extracting spectral dynamics from single chromophores in solution. *Phys. Rev. Lett.* **105**, 053005 (2010).
33. Brokmann, X., Bawendi, M., Coolen, L. & Hermier, J. P. Photon-correlation Fourier spectroscopy. *Opt. Express* **14**, 6333–6341 (2006).
34. Kuno, M., Fromm, D. P., Hamann, H. F., Gallagher, A. & Nesbitt, D. J. ‘On’/‘off’ fluorescence intermittency of single semiconductor quantum dots. *J. Chem. Phys.* **115**, 1028–1040 (2001).
35. Empedocles, S. A., Neuhauser, R., Shimizu, K. & Bawendi, M. G. Photoluminescence from single semiconductor nanostructures. *Adv. Mater.* **11**, 1243–1256 (1999).
36. Brokmann, X. *et al.* Statistical ageing and nonergodicity in the fluorescence of single nanocrystals. *Phys. Rev. Lett.* **90**, 120601 (2003).
37. Chung, I. H. & Bawendi, M. G. Relationship between single quantum-dot intermittency and fluorescence intensity decays from collections of dots. *Phys. Rev. B* **70**, 165304 (2004).
38. Nair, G., Zhao, J. & Bawendi, M. G. Biexciton quantum yield of single semiconductor nanocrystals from photon statistics. *Nano Lett.* **11**, 1136–1140 (2011).
39. Park, Y. S. *et al.* Near-unity quantum yields of biexciton emission from CdSe/CdS nanocrystals measured using single-particle spectroscopy. *Phys. Rev. Lett.* **106**, 187401 (2011).
40. Zhao, J., Chen, O., Strasfeld, D. B. & Bawendi, M. G. Biexciton quantum yield heterogeneities in single CdSe (CdS) core (shell) nanocrystals and its correlation to exciton blinking. *Nano Lett.* **12**, 4477–4483 (2012).
41. Spinicelli, P. *et al.* Bright and grey states in CdSe–CdS nanocrystals exhibiting strongly reduced blinking. *Phys. Rev. Lett.* **102**, 136801 (2009).
42. Cichos, F., von Borczyskowski, C. & Orrit, M. Power-law intermittency of single emitters. *Curr. Opin. Colloid Interface Sci.* **12**, 272–284 (2007).
43. Gomez, D. E., Califano, M. & Mulvaney, P. Optical properties of single semiconductor nanocrystals. *Phys. Chem. Chem. Phys.* **8**, 4989–5011 (2006).
44. Ghosh, Y. *et al.* New insights into the complexities of shell growth and the strong influence of particle volume in nonblinking ‘giant’ core/shell nanocrystal quantum dots. *J. Am. Chem. Soc.* **134**, 9634–9643 (2012).
45. Malko, A. V. *et al.* Pump-intensity- and shell-thickness-dependent evolution of photoluminescence blinking in individual core/shell CdSe/CdS nanocrystals. *Nano Lett.* **11**, 5213–5218 (2011).
46. Gomez, D. E., van Embden, J., Jasieniak, J., Smith, T. A. & Mulvaney, P. Blinking and surface chemistry of single CdSe nanocrystals. *Small* **2**, 204–208 (2006).
47. *CRC Handbook of Chemistry and Physics* 85th edn (CRC, 2005).
48. Bardou, F., Bouchaud, J. P., Aspect, A. & Cohen-Tannoudji, C. *Levy Statistics and Laser Cooling* (Cambridge Univ. Press, 2001).
49. Lee, S. F. & Osborne, M. A. Brightening, blinking, bluing and bleaching in the life of a quantum dot: Friend or foe? *Chem. Phys. Chem.* **10**, 2174–2191 (2009).
50. Zhang, J., Campbell, R. E., Ting, A. Y. & Tsien, R. Y. Creating new fluorescent probes for cell biology. *Nature Rev. Mol. Cell Biol.* **3**, 906–918 (2002).
51. Brown, E. B. *et al.* *In vivo* measurement of gene expression, angiogenesis and physiological function in tumours using multiphoton laser scanning microscopy. *Nature Med.* **7**, 864–868 (2001).
52. Liu, W. *et al.* Compact biocompatible quantum dots via RAFT-mediated synthesis of imidazole-based random copolymer ligand. *J. Am. Chem. Soc.* **132**, 472–483 (2010).

### Acknowledgements

The work received support from the NIH through grants 5-U54-CA119349 (M.G.B.) and 5R01CA126642 (M.G.B., D.F., R.K.J.), the ARO through the Institute for Soldier Nanotechnologies (W911NF-07-D-0004), and the NSF through a Collaborative Research in Chemistry Program (CHE-0714189) (M.G.B.). This work made use of the MRSEC Shared Experimental Facilities at MIT, supported by the National Science Foundation under award number DMR-08-19762 and the MIT DCIF NMR spectrometer funded through National Science Foundation Grants CHE-9808061 and DBI-9729592.

### Author contributions

O.C. and M.G.B. conceived and designed the project. O.C. performed the bulk of the experimental work with help from J.Z., V.P.C., J.C., C.W., D.K.H., H.W. and H-S.H. The data was analysed by O.C., J.Z., V.P.C., J.C., C.W. and M.G.B. All authors discussed the results and took part in producing the manuscript.

### Additional information

Supplementary information is available in the [online version of the paper](#). Reprints and permissions information is available online at [www.nature.com/reprints](http://www.nature.com/reprints). Correspondence and requests for materials should be addressed to M.G.B.

### Competing financial interests

The authors declare no competing financial interests.